Initial results of *in vivo* non-invasive cancer imaging in the human breast using near-infrared photoacoustics

Srirang Manohar[1*], Susanne E. Vaartjes[1], Johan C. G. van Hespen[1], Joost M. Klaase[2], Frank M. van den Engh[3], Wiendelt Steenbergen[1], and Ton G. van Leeuwen[1,4]

[1]*Institute for Biomedical Technology (BMTI), Biophysical Engineering Group, Faculty of Science and Technology, University of Twente, P.O. Box 217, 7500AE, Enschede, The Netherlands.*
[2]*Department of Surgery, Medisch Spectrum Twente, P.O. Box 50000, 7500KA, Enschede, The Netherlands.*
[3]*Department of Radiology, Medisch Spectrum Twente, P.O. Box 50000, 7500KA, Enschede, The Netherlands.*
[4]*Laser Center, Academic Medical Center, University of Amsterdam, P.O. Box 227700, 1100 DE Amsterdam, The Netherlands.*
[*]*Corresponding author:* s.manohar@utwente.nl

Abstract: Near-infrared photoacoustic images of regions-of-interest in 4 of the 5 cases of patients with symptomatic breasts reveal higher intensity regions which we attribute to vascular distribution associated with cancer. Of the 2 cases presented here, one is especially significant where benign indicators dominate in conventional radiological images, while photoacoustic images reveal vascular features suggestive of malignancy, which is corroborated by histopathology. The results show that photoacoustic imaging may have potential in visualizing certain breast cancers based on intrinsic optical absorption contrast. A future role for the approach could be in supplementing conventional breast imaging to assist detection and/or diagnosis.

OCIS codes: (170.5120) Photoacoustic imaging; (170.3830) Mammography; (170.3880) Medical and biological imaging; (170.1610) Clinical applications; (170.7170) Ultrasound.

References and Links

1. D. M. Parkin, F. Bray, J. Ferlay and P. Pisani, "Global Cancer Statistics, 2002," C. A. Cancer J. Clin. **55**, 74-108 (2005).
2. S. J. Nass, I. C. Henderson and J. C. Lashof, *Mammography and Beyond: Developing Technologies for the Early Detection of Breast Cancer* (National Academy Press, 2001).
3. M. A. Franceschini, K. T. Moesta, S. Fantini, G. Gaida, E. Gratton, H. Jess, W. W. Mantulin, M. Seeber, P. M. Schlag and M. Kaschke, "Frequency-domain techniques enhance optical mammography: Initial clinical results," PNAS **94**, 6468-6473 (1997).
4. D. Grosenick, H. Wabnitz, H. H. Rinneberg, K. T. Moesta and P. M. Schlag, "Development of a time domain optical mammograph and first *in vivo* applications," Appl. Opt. **38**, 2927–2943 (1999).
5. P. Carmeliet and R. K. Jain, "Angiogenesis in cancer and other diseases," Nature **407**, 249-257 (2000).
6. P. Vaupel, F. Kallinowski and P. Okunieff, "Blood Flow, Oxygen and Nutrient Supply, and Metabolic Microenvironment of Human Tumors: A Review," Cancer Res. **49**, 6449-6465 (1989).
7. B. J. Tromberg, N. Shah, R. Lanning, A. Cerussi, J. Espinoza, T. Pham, L. Svaasand and J. Butler, "Non-invasive *in vivo* characterization of breast tumors using photon migration spectroscopy," Neoplasia **2**, 26-40 (2000).
8. B. W. Pogue, S. P. Poplack, T. O. McBride, W. A. Wells, K. S. Osterman, U. L. Osterberg and K. D. Paulsen, "Quantitative Hemoglobin Tomography with Diffuse Near-Infrared Spectroscopy: Pilot Results in the Breast," Radiology **218**, 261-266 (2001).
9. M. Xu and L. V. Wang, "Photoacoustic imaging in biomedicine," Rev. Sci. Instrum. **77**, 041101 (2006).
10. A. A. Oraevsky, E. V. Savateeva, S. V. Solomatin, A. A. Karabutov, V. G. Andreev, Z. Gatalica, T. Khamapirad and P. M. Henrichs, "Optoacoustic imaging of blood for visualization and diagnostics of breast cancer," Proc. SPIE **4618**, 81-94 (2002).
11. T. Khamapirad, P. M. Henrichs, K. Mehta, T. G. Miller, A. T. Yee and A. A. Oraevsky, "Diagnostic imaging of breast cancer with LOIS: clinical feasibility," Proc. SPIE **5697**, 35-44 (2005).
12. R. A. Kruger, K. D. Miller, H. E. Reynolds, W. L. Kiser Jr., D. R. Reinecke, G. A. Kruger, "Breast Cancer *in vivo*: Contrast Enhancement with Thermoacoustic CT at 434 MHz-Feasibility Study," Radiology **216**, 279-283 (2000).

#85676 - $15.00 USD Received 25 Jul 2007; revised 3 Sep 2007; accepted 10 Sep 2007; published 12 Sep 2007

13. S. Manohar, A. Kharine, J. C. G. van Hespen, W. Steenbergen and T. G. van Leeuwen, "The Twente Photoacoustic Mammoscope: system overview and performance," Phys. Med. Biol. **50** 2543-2557 (2005).
14. S. Manohar, A. Kharine, J. C. G. van Hespen, W. Steenbergen and T. G. van Leeuwen, "Photoacoustic mammography laboratory prototype: imaging of breast tissue phantoms," J. Biomed. Opt. **9**, 1172-1181 (2004).
15. F. A. Duck, *Physical Properties of Tissue* (Academic Press, 1990).
16. L. Spinelli, A. Torricelli, A. Pifferi, P. Taroni, G. M. Danesini and R. Cubeddu, "Bulk optical properties and tissue components in the female breast from multiwavelength time-resolved optical mammography," J. Biomed. Opt. **9**, 1137-1142 (2004).
17. T. P. Padera, B. R. Stoll, J. B. Tooredman, D. Capen, E. Di Tomaso and R. K. Jain, "Cancer cells compress intratumour vessels," Nature **427**, 695 (2004).
18. M. Sarntinoranont, F. Rooney and M. Ferrari, "Interstitial stress and fluid pressure within a growing tumor," Ann. Biomed. Eng. **31**, 327-335 (2003).
19. J. Holash, P. C. Maisonpierre, D. Compton, P. Boland, C. R. Alexander, D. Zagzag. G. D. Yancopoulos and S. J. Wiegand, "Vessel cooption, regression, and growth in tumors mediated by angiopoietins and VEGF," Science **284**, 1994-1998 (1999).
20. G. D. Yancopoulos, S. Davis, N. W. Gale, J. S. Rudge, S. J. Wiegand and J. Holash, "Vascular-specific growth factors and blood vessel formation," Nature **407**, 242-248 (2000).
21. R. Matsubayashi, Y. Matsuo, G. Edakuni, T. Satoh, O. Tokunaga and S. Kudo, "Breast Masses with Peripheral Rim Enhancement on Dynamic Contrast-enhanced MR Images: Correlation of MR Findings with Histologic Features and Expression of Growth Factors," Radiology **217**, 841-848 (2000).
22. J. Laufer, D. Delpy, C. Elwell and P. Beard, "Quantitative spatially resolved measurement of tissue chromophore concentrations using photoacoustic spectroscopy:application to the measurement of blood oxygenation and haemoglobin concentration," Phys. Med. Biol. **52**, 141-168 (2007).

1. Introduction

The breast is the site of the highest incidence of cancer among women worldwide and especially in the affluent world regions. At the current rates of incidence, it is estimated that 1.4 million new cases will be uncovered in 2010 [1]. Globally breast cancer accounts for the highest malignancy-associated deaths among women, with over 400,000 in 2002 [1]. Detection and diagnosis of breast cancer is usually based on x-ray mammography, ultrasound imaging and biopsy. While high accuracies are possible with this triple assessment, there are drawbacks in both imaging modalities. X-ray mammography misses cancers and also has a high rate of false positive results [2]. These limitations occur principally in radiodense glandular breasts which see poor interpretation and reduced accuracies. Further, concerns regarding the use of ionizing radiation and patient discomfort have been expressed. Ultrasonography plays an adjunctive role to x-ray imaging in solid mass-cyst differentiation but developments are still early for any large-scale applications in differentiating malignant from benign abnormalities [2].

The burden of breast cancer on society and the shortcomings of clinical breast imaging have been the impelling forces for the quest in developing alternative imaging techniques that address the limitations of the current technologies. NIR optical imaging is one such promising technique that avoids ionizing radiation, is relatively inexpensive and does not require severe breast compression [3,4]. The source of optical contrast between cancer and non-pathological tissue arises in the enhanced vascularity of the lesion due to angiogenesis [5,6]; hemoglobin and oxy-hemoglobin in blood are the principal absorbers in the NIR spectrum up to 900 nm. In optical imaging the incident energy is in the form of photons and detected energy comprises those photons that have escaped absorption during their interaction with tissue. Using models of photon propagation in tissue, the detected photons are interpreted in terms of the absorption properties in the breast; higher absorption taken as a signature of a vascularised tumor [7, 8]. However, since photons are strongly scattered in tissue, spatial resolution is generally poor. Thus, while optical imaging precludes the detection and analysis of absorbed photons, the photoacoustic (also referred to as optoacoustic) technique on the contrary depends precisely on these absorbed photons for a signal [9]. The absorbed photons undergo thermalization, creating localized temperature increase and consequently thermal expansion at absorbing sites; when pulsed light is used pressure transients result which can be detected using conventional ultrasound detectors at the surface of tissue. The spatial distribution of absorbing structures can be determined by analyzing the propagation times of the ultrasound

#85676 - $15.00 USD Received 25 Jul 2007; revised 3 Sep 2007; accepted 10 Sep 2007; published 12 Sep 2007

transients at a plurality of detector positions. Since ultrasound scatters 2-3 orders of magnitude lower than light in soft tissue, photoacoustic imaging can offer high resolution [9]. The application of NIR photoacoustics for breast imaging has been reported by Oraevsky and co-workers [10, 11] in the laser optoacoustic imaging system (LOIS) but the technique is as yet in its infancy. In a radiofrequency (RF) counterpart of NIR photoacoustics, Kruger and co-workers [12] used radiation of 434 MHz frequency for excitation in the thermoacoustic computed tomography (TCT) scanner to probe RF absorption by ionic water associated with human breast cancer.

Our NIR photoacoustic mammoscope (PAM) uses 5 ns width laser pulses at a wavelength of 1064 nm for excitation and a flat ultrasound sensor matrix for detection. We present the salient features of the instrument and the first results of a pilot study to ascertain the feasibility of using NIR photoacoustics to detect tumors in the breasts of human patients.

2. Materials and methods

2.1 Patients

The study protocol was approved by the Medical Ethics Committee (METC) of the Medisch Spectrum Twente, Enschede. Patients with a palpable lump in the breast after entry level examination suspect for malignancy were included in the study. An exclusion criterion was history of core-needle biopsy larger than 1 mm in diameter within a period of 6 months prior to the study. Written consent of patients was obtained after ensuring that they had understood the implications of participating in the study.

2.2 X-ray and ultrasound imaging

Diagnostic x-ray imaging was performed in two views, craniocaudal (CC) and mediolateral oblique (MLO) using the Selenia Full Field Digital Mammography System (Hologic, Bedford, USA). Breast sonography was performed in sagittal and transversal scanning planes using a Philips iU22 ultrasound system (Philips Medical Systems, Best, The Netherlands) equipped with a L12-5 50 mm linear probe operated at 12 MHz. The x-ray and echo mammograms were interpreted by a dedicated breast imaging radiologist (F.M.vd.E).

2.3 The Photoacoustic Mammoscope (PAM)

Figure 1 shows photographs of the instrument. Some important specifications of PAM are consolidated in Table 1; further details including system performance on liquid and solid phantoms may be found elsewhere [13,14].

The patient-instrument interface is a hospital bed [14], the instrument mounted on the frame of the bed below. The subject lies prone on the bed with her suspect breast pendant through the aperture (a). Under the bed, the breast is compressed mildly between the detector matrix (b) and the glass plate (c) of a compartment (d) that carries the scanning system. Acoustic coupling gel is used between the breast and ultrasound detector. The detector has 590 active elements which can be activated one at a time. The laser (e) is mounted at the bottom of the bed and coupled to a light delivery system [14] whose output is coupled to the scanning system. A photoacoustic scan is performed around the region which is expected to harbor the tumor by setting the scanning system to translate the laser beam in steps across breast through the glass window. For every position of the laser beam on the breast, an antipodal element on the detector is activated. The diameter of the beam (16 mm) and the scattering of light in the breast will ensure that acoustic sources in the breast will be present in the overlapping reception cones of neighboring detection elements so that the delay-sum algorithm can be applied. A laser fluence rate not greater than 30 mJ/cm^2 is applied, which does not exceed the maximum permissible exposure (MPE) for this class of laser with detector element signals being averaged over 100 pulses.

#85676 - $15.00 USD Received 25 Jul 2007; revised 3 Sep 2007; accepted 10 Sep 2007; published 12 Sep 2007

Fig. 1. The Twente Photoacoustic Mammoscope. a – aperture to insert breast, b – ultrasound detector matrix, c – glass window of d – scanning system compartment, e – Q-switched Nd:YAG laser operated at 1064 nm with 5 ns pulses, f – laser safety curtain which is drawn around the instrument during the measurement, g – interface electronics between detector and computer, h – linear stage carrying detector matrix driven by handwheel to apply mild compression to breast, I – laser remote control unit, j – laser power supply.

Table 1. Specifications of the Photoacoustic Mammoscope

Laser[a]	Wavelength	1064 nm
	Pulse width	5 ns
	Repetition rate	10 Hz
Detector[b]	Matrix shape	circular
	Matrix size	90 mm diameter
	Number of elements	590
	Element size	2x2 mm
	Element pitch	3.175 mm
	Central frequency	1 MHz
	Bandwidth	130 %
Reconstruction	Algorithm	Phase-array[c]
	Lateral resolution[d]	2.3-3.9 mm
	Axial resolution[d]	2.5-3.3 mm

[a]Brilliant B, Quantel (Paris, France)
[b]Lunar Corporation, General Electric (Wisconsin, Madison, USA)
[c]Synonymous with delay and sum algorithm
[d]For depths between 15 and 60 mm

2.4 Photoacoustic imaging protocol

PAM was set up in the Breast Care facility of the hospital. Entry level examinations of patients at the facility comprise clinical examination, x-ray mammography and breast sonography. When the breast is suspicious for malignancy, the photoacoustic scan is performed before a biopsy of the lesion is made for histological assessment. The photoacoustic examination comprises a craniocaudal (CC) view of the region-of-interest (ROI) of the suspect breast.

The same clinician who performed the x-ray or ultrasound examination positioned the breast between the glass window of the scanning system compartment and the ultrasound detector, so that photoacoustic imaging was performed principally in the area which harbors the tumor. Mild compression was applied to the breast by manually turning the handwheel (Fig. 1) that drives the carriage holding the detector towards the glass window of the scanning system compartment. Copious amounts of acoustic coupling gel were used between breast and detector. At the instant the patient indicated any discomfort during the gradual application of pressure, further application of compression was terminated. The patient was then expected to lie immobile in this position for the scan period. The scan size was chosen large enough to accommodate sufficient non-pathological tissue, under the condition that the measurement

#85676 - $15.00 USD Received 25 Jul 2007; revised 3 Sep 2007; accepted 10 Sep 2007; published 12 Sep 2007

time did not exceed 45 minutes; the average scan time was 30 minutes. The step-size of scanning the laser beam was set equal to the inter-element spacing of the detector matrix.

2.5 Photoacoustic image reconstruction and analysis.

Images were reconstructed off-line using a phase-array approach to focus the sensitivity of the detectors in the planar matrix to voxels in turn, into which the investigated volume is assumed to be divided. The algorithm is formulated as:

$$S^V(t) = \frac{\sum_i w_i^V \left[S_i(t) h(t + \tau + \delta_i^V) \right]_{|\max - \min|}}{\sum_i w_i^V}, \quad (1)$$

where w_i^V is a weight-factor which accounts for angular sensitivity of the detector, $S_i(t)$ is the signal, δ_i^V the delay applied, with i a specific detector element and V a specific voxel. The window function with width τ is defined by:

$$h(t+\tau) = \begin{cases} 1 \text{ for } |t| \le \tau/2 \\ 0 \text{ otherwise} \end{cases} \quad (2)$$

In practice, a sliding window $h(t)$ with width τ operates on each signal trace, the position of this window given by the delay δ_i^V which is determined by the distance between a voxel to the detector element considered divided by acoustic velocity. Within this window the peak-peak value of the signal is determined. These values for all elements are then summed up and assigned to the voxel.

The acoustic velocity required to perform the delay operation was chosen to be 1.45 mm/μs [15]. The large signal from the breast surface was excluded from signal traces in the reconstruction. Typically voxel sizes of 0.5 mm and window sizes of 5 mm were used. The reconstructed data was filtered using a three-point median filter and normalized to [0..255]. The reconstruction was visualized using either slice planes or maximum-intensity projections (MIPs) through the three-dimensional volume.

Contour lines at a threshold intensity value based on the standard deviation of the photoacoustic MIP image were superposed as black dotted lines on the MIP images. The threshold level was obtained as $\mu+\sigma$, where μ is the mean value and σ is the standard deviation of the image.

3. Results

At the time of going to press, 13 patients have participated in the study. Seven of these measurements were not acceptable for further analysis due to the following reasons:

1) Tumor not present in scan area due to
    a) Incorrect operator setting of scanning region coordinates (1 patient)
    b) Small breast size or occurrence of ROI too close to chest wall (3 patients)
2) Erroneous signals measured due to poor acoustic contact between breast and detector due to a combination of insufficient compression of breast, insufficient amount of gel and occurrence of ROI close to the lateral edge of breast in CC view. (3 patients)

The unacceptable measurements were discovered either during or immediately after the scans and the results not considered for further investigations. Most of these cases occurred during the early part of the study. Of the 6 technically acceptable measurements, 5 were on suspect breasts and 1 was on a breast with a cyst. We discuss the results of 2 of the 5 suspect cases.

#85676 - $15.00 USD Received 25 Jul 2007; revised 3 Sep 2007; accepted 10 Sep 2007; published 12 Sep 2007

3.1 Case 1

Case 1 (patient 01574983, MST) refers to a 50 year old Caucasian woman with a palpable abnormality in the right breast at 11 'O' clock, which was verified post-surgery as an infiltrating ductal carcinoma. X-ray mammography [Fig. 2(a)] revealed a cluster of microcalcifications within a region of architectural distortion with spiculation. Breast sonography [Fig. 2(b)] showed an irregularly marginated solid hypoechoic mass (major axis 17 mm). The lesion was highly suspect for malignancy and a core biopsy was recommended.

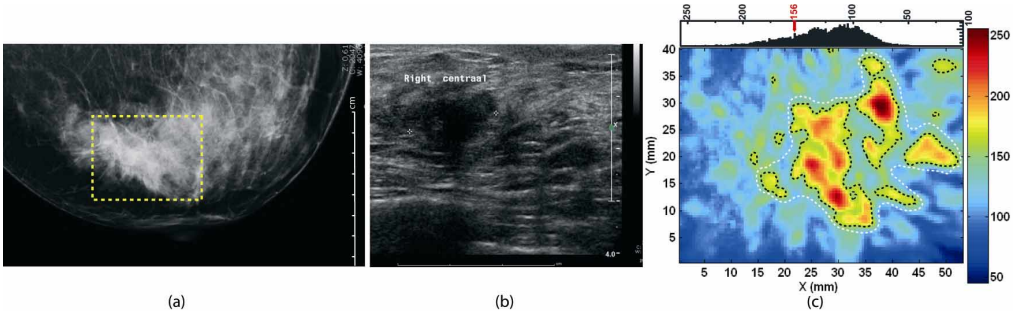

Fig. 2. Case 1 of 50 year old woman with invasive ductal carcinoma in right breast. (a) Craniocaudal x-ray mammogram reveals architectural distortion with spiculations. Window shows expected location of the ROI for the photoacoustic scan. (b) Transverse sonographic scan image shows 17 mm irregular hypoechoic solid mass. (c) Craniocaudal photoacoustic MIP image in top-view reveals higher intensity regions attributed to tumor vascularization. Contour lines (black dotted) are drawn using the level indicated in the image histogram above. The possible extent of the tumor mass (major axis 35 mm) is indicated by the white dotted line encompassing the cluster of vascular regions. The photoacoustic image cannot be compared point by point with the x-ray image in ROI due to differences in compression and in ROI positioning.

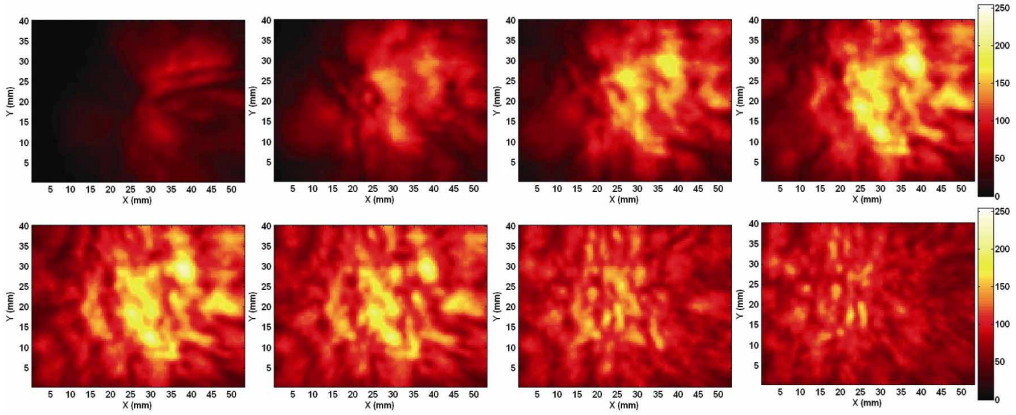

Fig. 3. Case 1 of 50 year old woman with invasive ductal carcinoma in right breast. Montage of selected slice images of photoacoustic reconstructed data set in craniocaudal view. The inter-slice spacing is 1.5 mm with the first slice 6.5 mm below the illuminated breast surface and the last 17 mm. High intensity regions correspond to vascular 'hot spots'.

At this point we imaged the breast using the PAM, in the ROI with the tumor expected to lie in the center of the scan area of 53x40 mm corresponding to 17x13 detection elements. The breast thickness under light compression applied in the PAM was measured to be 50 mm. Regions of higher intensity are identifiable clustered together in the photoacoustic maximum intensity projection (MIP) image [Fig. 2(c)] and slice plane images (Fig. 3). A white dotted line is drawn in the MIP image [Fig. 2(c)] as guide to the eye enclosing the cluster of contiguous higher-intensity zones defined by contour lines; the major axis of this cluster is 35

#85676 - $15.00 USD Received 25 Jul 2007; revised 3 Sep 2007; accepted 10 Sep 2007; published 12 Sep 2007

mm. An average image contrast of 1.45 is calculated as the ratio of mean pixel values within and outside the white boundary.

3.2 Case 2

Case 2 (patient 06166651, MST) refers to a Caucasian woman of 57 years with a palpable mass in her right breast which was pathologically verified after surgical intervention as a carcinoma with neuroendocrine differentiation. The x-ray image [Fig. 4(a)] reveals a fairly dense oval mass (40 mm on the major axis) centrally located behind the nipple with predominantly circumscribed margins.

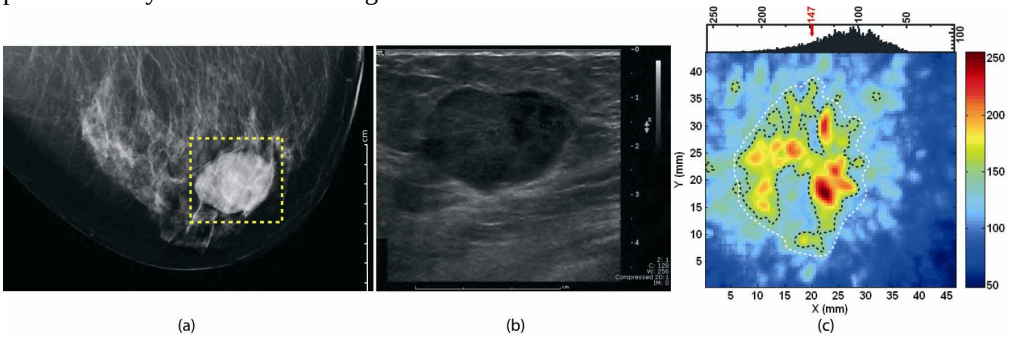

Fig. 4. Case 2 of 57 year old woman with invasive ductal carcinoma exhibiting neuroendocrine differentiation in right breast. Gross features in craniocaudal x-ray mammogram (a) and transverse sonographic scan image (b) indicate benignity, but presence of microcalcifications in (a) and age of patient prompted core biopsy. Craniocaudal photoacoustic MIP image (c) in ROI (red window in x-ray mammogram) shows high intensity distributions in a ring shape attributable to higher vascular densities at tumor periphery. Contour lines (black dotted) are superposed using level indicated in the image histogram above. The photoacoustic image cannot be compared point by point with the x-ray image in ROI due to differences in compression and in ROI positioning.

A number of microcalcifications (around 10) of varying sizes and shapes appear laterally in the tumor distributed regionally (a magnified image is shown in Fig. 5). The breast sonogram [Fig. 4(b)] reveals a uniformly hypoechoic circumscribed tumor (major axis 32 mm) with a few anechoic regions suggestive of cystic features. A mild posterior enhancement is visible and a diffuse offshoot is seen on the medial side of the mass. While there are a number of benign indicators in the x-ray and ultrasound images, primarily the presence of heterogeneous calcifications (at least 2 with a linear aspect) in the x-ray images but also the age of the patient prompted the radiologist to treat the lesion as suspicious and a core-biopsy was recommended.

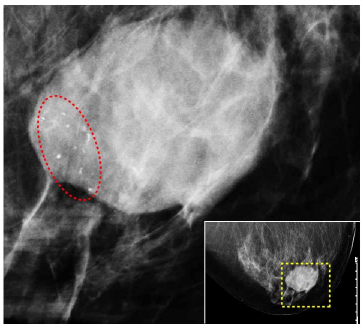

Fig. 5. Magnified region-of-interest of craniocaudal x-ray mammogram (inset) of Case 2. Image shows oval mass with predominantly circumscribed borders with a small number of irregular microcalcifications within dotted red oval.

#85676 - $15.00 USD Received 25 Jul 2007; revised 3 Sep 2007; accepted 10 Sep 2007; published 12 Sep 2007

The photoacoustic scan window covered 46x43 mm corresponding to 15x14 detection elements. Breast thickness in the scanner was measured to be 59.5 mm. In the photoacoustic MIP image [Fig. 4(c)] and slice images (Fig. 6) a pronounced ring-shaped structure of higher intensity due to higher optical absorption is seen. The outer diameter along the major axis of the ring structure (30 mm) is close to the sonographically determined lesion size and the pathologically estimated carcinoma size (26 mm). The average image contrast within the white boundary is calculated to be 1.55.

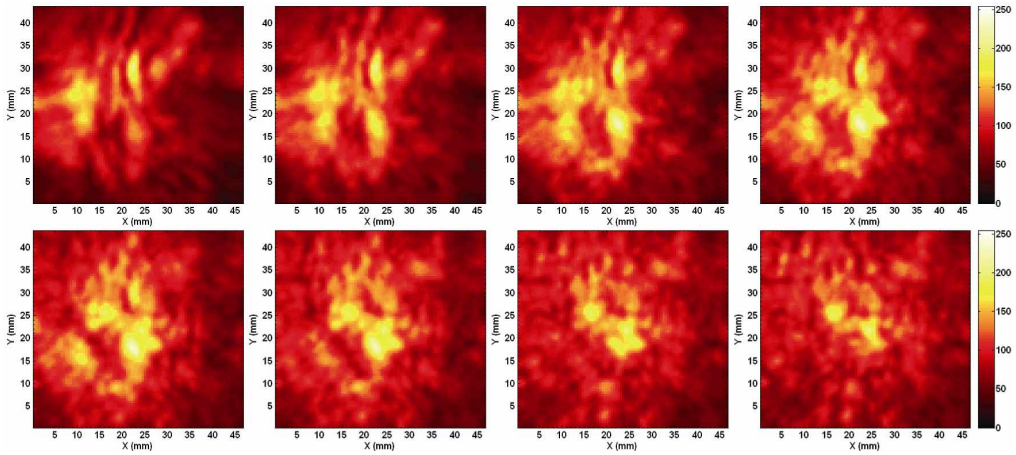

Fig. 6. Case 2 of 57 year old woman with invasive ductal carcinoma exhibiting neuroendocrine differentiation in right breast. Selected slice images of photoacoustic reconstructed data set in craniocaudal view. The inter-slice spacing is 1 mm with the first slice 9.5 mm below the illuminated breast surface. The ring pattern of higher intensity which depicts strong vascularization at the tumor periphery is evident in the slices at depths 11.5 to 14.5 mm

4. Discussion

4.1 Case 1

At 1064 nm the principal chromophores in the breast are lipids, oxy-hemoglobin, hemoglobin and water [16]. The clustering of the regions of higher absorption where we expect the tumor to reside leads us to believe that we are seeing predominantly the presence of total hemoglobin. We thus attribute the areas of higher intensity in the photoacoustic images to blood content in the heterogeneous distribution of vascularization associated with cancer [6]. The disorganized vascular distribution appears consistent with the irregular features in the x-ray mammogram and ultrasound images. [Fig. 2(a) and Fig. 2(b)]

The white dotted line in the MIP image [Fig. 2(c)] thus encloses vascular zones and may be construed as the tumor extent. The major axis of this cluster (35 mm) is an estimate of the carcinoma size which though larger than the sonographically estimated size matches the pathologic size (32 mm) of the carcinoma.

4.2 Case 2

We believe that the remarkable ring pattern (Fig. 4(c) and Fig. 6) depicts vascular distribution in the tumor; the periphery of the tumor is the cancer invasion front with rapid cell proliferation and accompanying robust angiogenesis. The lower central vascularity can have its explanation in the observation that intratumor vasculature undergoes compression and collapse due to mechanical forces exerted by proliferating cancer cells [17], with greater compressive stresses predicted [8] at the interior of the tumor compared with the margins. In such a scenario the interior of a tumor suffers impaired vascular function with diminished blood perfusion while the peripheral vasculature remains viable as observed in the photoacoustic images. The ring-shaped pattern is also consistent with a tumor angiogenesis model [19,20] that postulates a dynamic balance between blood vessel regression and growth

#85676 - $15.00 USD Received 25 Jul 2007; revised 3 Sep 2007; accepted 10 Sep 2007; published 12 Sep 2007

mediated by vascular-specific growth factors. Certain tumors begin as vascular masses when they commandeer existing host vessels. In response to this inappropriate co-option, the host vessels mount a defence whereby they regress by apoptosis. This leaves an avascular and hypoxic mass which leads to extensive tumor cell death. The remaining tumor is ultimately resuscitated by strong angiogenesis at the tumor margin [19,20]. Finally, ring patterns have been reported in dynamic magnetic resonance (MR) imaging of contrast agent uptake in breast carcinomas [21] with rim enhancement correlating well with ratios of tumor periphery-core microvessel densities. It is noteworthy that the photoacoustic images of Case 2 reveal similar vascular morphological features based simply on intrinsic contrast.

5. Concluding remarks

The initial results of the study are exciting: in 4 of the 5 cases photoacoustic images revealed regions of higher absorption in ROIs attributable to tumor vascularization. Case 2 is an interesting case because of the number of benign indicators associated with the radiological images while photoacoustic images suggested malignancy. This case illustrates the potential of the approach but also gives an impression of the conceivable utility of the technique in breast evaluation in the future. Photoacoustics can "see" vascular features associated with cancer which could impact detection and/or diagnosis but which are not revealed by x-rays and ultrasound.

However, the technique is as yet nascent and there are many unresolved issues. On the technical side multi-element readout ultrasound detector matrices with high sensitivity and wide frequency bandwidths are required to reduce measurement times and make full-breast scans possible. Quantitative spectroscopic imaging [8,22] is required for defining cancer physiology relevant features related to oxygen saturation. On a fundamental level an outstanding biological question is: Are features related to vascularization reliable detection/diagnostic characteristics of malignancy? Carefully designed clinical studies comparing various imaging modalities supported by technical innovations will be required to answer this and other questions. This knowledge would help to define the exact value that photoacoustic mammography can furnish to breast cancer detection and/or diagnosis.

Acknowledgments

S. Manohar is supported in the Vernieuwingsimpuls program (TTF.6527) by the Netherlands Organisation of Scientific Research (NWO) and the Technology Foundation (STW). The authors acknowledge Prof. Dr. G. J. den Heeten and Prof. V. Subramaniam for comments on the manuscript; Dr. A. K. H. Thé for discussions; Dr. F. F. M. de Mul and Dr. H. J. C. M. Sterenborg for suggestions and Dr. A. Stam for maintaining patient records. Nursing staff of the Breast Care facility of the Medisch Spectrum Twente are acknowledged for cooperation and help during photoacoustic measurements.

#85676 - $15.00 USD Received 25 Jul 2007; revised 3 Sep 2007; accepted 10 Sep 2007; published 12 Sep 2007